Front. Optoelectron. 2018, 11(2): 148–154
https://doi.org/10.1007/s12200-018-0809-x

RESEARCH ARTICLE

Franson interferometry with a single pulse

Eric Y. ZHU (✉)[1], Costantino CORBARI[2], Alexey V. GLADYSHEV[3], Peter G. KAZANSKY[2], Li QIAN[1]

1 Department of Electrical and Computer Engineering, University of Toronto, Toronto, ON M5S 3G4, Canada
2 Optoelectronics Research Centre, University of Southampton, Southampton SO17 1BJ, UK
3 Fiber Optics Research Center of the Russian Academy of Sciences, Moscow 119333, Russia

Abstract In classical optics, interference occurs between two optical fields when they are indistinguishable from one another. The same holds true in quantum optics, where a particular experiment, the Franson interferometer, involves the interference of a photon pair with a time-delayed version of itself. The canonical version of this interferometer requires that the time delay be much shorter than the coherence length of the pump used to generate the photon pair, so as to guarantee indistinguishability. However, when this time delay is comparable to the coherence length, conventional wisdom suggests that interference visibility degrades significantly. In this work, though, we show that the interference visibility can be restored through judicious temporal post-selection. Utilizing correlated photon pairs generated by a pump whose pulsewidth (460 ps) is shorter than the interferometer's time delay (500 ps), we are able to observe a fringe visibility of 97.4±4.3%. We believe this new method can be used for the encoding of high-dimensional quantum information in the temporal domain.

Keywords quantum optics, quantum interference, nonlinear optics, optical fibers

1 Introduction

Which-way interference is a crucial concept in our understanding of quantum optics. Put simply, it states that if a process gives rise to individual states that are indistinguishable from one another, the resultant wavefunction must be described as a superposition of those individual states.

Perhaps the quintessential demonstration of which-way interference is the Hong-Ou-Mandel (HOM) effect [1,2], where identical photons interfere at a 50/50 beam splitter (BS). As with classical optical interference, maximal visibility is observed when the spectral, temporal, and spatial modes, essentially all degrees of freedom, of the individual photons are perfectly overlapped. The result of the interference is that both photons will exit the same output port of the beam splitter; however, as both output ports are equivalent, the state generated as a result of the interference must be a superposition of two spatial modes:

$$|1\rangle_1|1\rangle_2 \xrightarrow{\text{BS}} \frac{1}{\sqrt{2}}(|2\rangle_3|0\rangle_4 + |0\rangle_3|2\rangle_4),$$

where $|k\rangle_l$ denotes k photons in port l of the BS, with ports 1 and 2 (3 and 4) denoting the inputs (outputs) of the BS.

In contrast to the HOM effect, where a photon pair interferes with itself, the Franson interferometer [3,4] involves the interference of a photon pair generated at one time with another (identical) photon pair generated at a later time. When the biphotons are generated from a parametric downconversion (PDC) source, this interference arises from the temporal indistinguishability of the photon pairs generated by a long coherence length pump. In effect, the PDC source generates a temporally-entangled biphoton state [5] of the form:

$$\begin{aligned}|\psi\rangle &= \int \mathrm{d}t_\mathrm{s}\mathrm{d}t_\mathrm{i} A(t_\mathrm{s},t_\mathrm{i})|t_\mathrm{s},t_\mathrm{i}\rangle \\ &= C\int \mathrm{d}t_\mathrm{s}\mathrm{d}t_\mathrm{i}\ \mathrm{e}^{-\Delta^2(t_\mathrm{s}-t_\mathrm{i})^2}\mathrm{e}^{-\left(\frac{t_\mathrm{s}+t_\mathrm{i}}{2\tau_\mathrm{h}}\right)^2}|t_\mathrm{s},t_\mathrm{i}\rangle, \end{aligned} \quad (1)$$

where $A(t_\mathrm{s},t_\mathrm{i})$ is the temporal biphoton wavefunction, t_s (t_i) is the time at which the signal (idler) photon of each pair is generated, Δ is the bandwidth of each individual photon, τ_h is the pump coherence time, and C is a normalization constant. While the bandwidth Δ of the photons generated is large (on the order of THz), the energies of the signal

Received February 2, 2018; accepted May 7, 2018

E-mail: eric.zhu@utoronto.ca

Invited Paper, Special Issue—Photonics Research in Canada

(ω_s) and idler (ω_i) photons of each pair must add up to that of the pump ($\omega_s+\omega_i= \omega_{pump}$). The large bandwidth is due to energy-time uncertainty as the idler and signal photons of each pair are generated almost simultaneously ($t_s \sim t_i$) in the PDC process.

The conventional experimental Franson scheme is shown in Fig. 1; a photon pair (drawn as red and green) is generated via parametric downconversion of a long coherence pump (blue). Each photon is then sent to two identical, but spatially separate, unbalanced Mach-Zehnder interferometers (MZIs) with temporal imbalance τ. When the coherence length τ_h of the pump laser is much longer than the MZI imbalance ($\tau_h >> \tau$), interference occurs between the probability amplitude of the pair of photons generated at time t and another pair of photons generated at $t+\tau$ due to their indistinguishability (Eq. (1)). This temporal entanglement (Eq. (1)) can be used to demonstrate the nonlocal interference aspects of quantum mechanics [3], and the violation of Bell's inequalities [6]. To prevent single photon interference at the output of the MZI, the value of τ is made much larger than the single photon correlation time τ_{cor}, which is related to its bandwidth $\Delta\left(\tau_{cor}\sim\frac{1}{\Delta}\right)$, giving a bound for τ:

$$\frac{1}{\Delta} \ll \tau \ll \tau_h. \tag{2}$$

While the original formulation [3] of the Franson interferometer used a long-coherence continuous wave (CW) pump to generate the entangled photon pairs (Eq. (1)), a pulsed equivalent has also been demonstrated. In this so-called time-bin entanglement [7], a coherent train of short pulses is used to pump a nonlinear medium to generate photon pairs that are entangled in discrete timeslots. The pulsetrain is often generated using a long-coherence CW pump, following by an intensity modulator and optical amplifier. The MZI imbalance τ used is an integer multiple of the pulsetrain period. Such a setup is experimentally complex, and prone to disturbances such as the timing jitter of the modulator's driving signal and the temperature fluctuation of the MZI.

In this work, we demonstrate yet another variation of the Franson interferometer. We use a transform-limited pulsed pump; however, unlike time-bin entanglement, we do not look at the interference of photon pairs generated by different pulses, but rather the interference of photon pairs generated by the same pulse (Fig. 2(a)). We will work in the regime where $\tau \sim \tau_h$, with τ_h now representing the characteristic temporal width of the pulse.

The motivation for using a pulsed pump is three-fold. First, it permits us to time-resolve the arrival times of both the signal and idler photons with respect to a common reference (the pump pulse), allowing for a new way to visualize the interference (Fig. 2). Second, this two-dimensional (2D) time-resolution enables the observation and recovery of Franson interference even when the pump pulsewidth τ_h is on the order of (or slightly shorter than) the MZI mismatch τ. And lastly, the 2D visualization gives us the ability to correct for detector jitter, a source of noise that would otherwise deleteriously lower the interference visibility.

One potential application of this work is the transmission of higher-dimensional (more than 1 qubit) quantum information into the temporal domain [8]. By interfering two different temporal portions of a pulsed biphoton (photon pair), the value of the encoded phase can be recovered.

In what follows, we show both computationally (Section 2) and experimentally (Section 3) that we can observe near-unity interference visibility with our Franson-like interferometer.

2 Theory and simulation

The interference that occurs in our interferometer can be explained qualitatively. The biphoton wavepacket generated by the downconversion of a transform-limited pump pulse has the same temporal extent (τ_h) as the pump (Eq. (1)). After traversing the MZIs, the probability amplitudes of the two temporally-displaced wavepackets overlap to give rise to interference in a small (shaded)

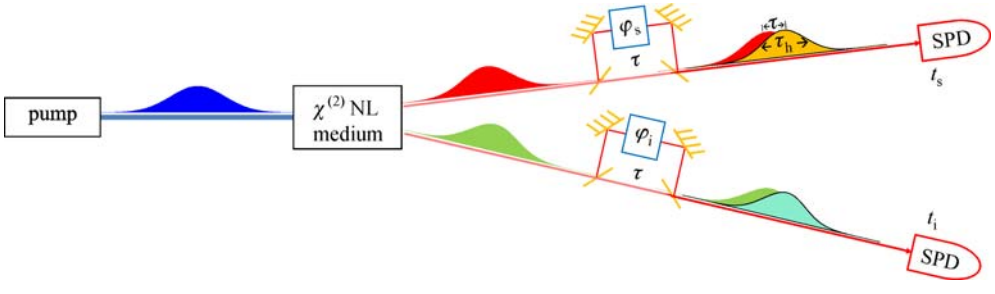

Fig. 1 Experimental setup for the standard Franson interferometer. A photon pair (red, green pulses) is generated inside a second-order nonlinear (NL) medium by a high energy pump (blue). Each photon in the pair is then sent through an unbalanced Mach-Zehnder interferometer (MZI) that adjusts the phase φ_s, φ_i of each photon independently. Coincidence measurements are performed using single photon detectors (SPDs) so that the photon arrival times (t_s, t_i) are measured

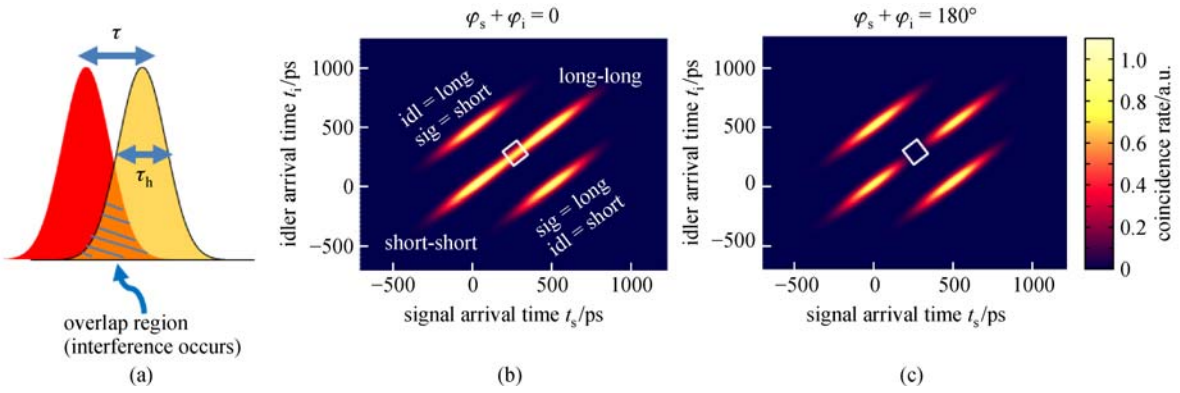

Fig. 2 (a) Interference between two photon pairs generated at the trailing and leading edges of the same pump pulse can occur when their temporal wavepackets overlap (shaded region). In (b) and (c), the simulated coincidence rates are plotted as a function of the signal and idler arrival times (t_s,t_i) using Eq. (4) and parameters given in Table 1. The white box in each plot corresponds to the shaded region in (a)

region (Fig. 2(a)). We note that interference is only observed when both photons in the photon pair traverse the same leg of their respective interferometers.

We can numerically simulate the interference by modeling the coincidence statistics as measured by single photon detectors (SPDs) at the outputs of the MZIs. The associated annihilation field operators are [5,9]

$$a_{\mathrm{SPD,signal}}(t_\mathrm{s}) = \frac{1}{2}[a_\mathrm{s}(t_\mathrm{s}) - \mathrm{e}^{\mathrm{i}\varphi_\mathrm{s}} a_\mathrm{s}(t_\mathrm{s}-\tau)], \tag{3a}$$

$$a_{\mathrm{SPD,idler}}(t_\mathrm{i}) = \frac{1}{2}[a_\mathrm{i}(t_\mathrm{i}) - \mathrm{e}^{\mathrm{i}\varphi_\mathrm{i}} a_\mathrm{i}(t_\mathrm{i}-\tau)], \tag{3b}$$

where $a_s(t)$ ($a_i(t)$) is the annihilation operator for the signal (idler) photon that traversed the short arm, and $a_s(t-\tau)$ ($a_i(t-\tau)$) is the annihilation operator for the signal (idler) photon that traversed the long arm of the MZI. The standard commutation relations $([a_J^+(t),a_K(t')] = \delta_{JK}\,\delta(t-t')$ for J,K = s,i) apply. As the interference is observed only when a coincidence measurement is performed, we can model the coincidence rate $R(t_s,t_i)$ as [9]

$$\begin{aligned} R(t_\mathrm{s},t_\mathrm{i}) &= \langle\psi| a^+_{\mathrm{SPD,idler}}(t_\mathrm{i}) a_{\mathrm{SPD,idler}}(t_\mathrm{i}) a^+_{\mathrm{SPD,signal}}(t_\mathrm{s}) a_{\mathrm{SPD,signal}}(t_\mathrm{s}) |\psi\rangle \\ &\sim \Bigg| \underbrace{A(t_\mathrm{s},t_\mathrm{i})}_{\substack{\text{signal = short arm}\\ \text{idler = short arm}}} + \underbrace{\mathrm{e}^{\mathrm{i}(\varphi_\mathrm{s}+\varphi_\mathrm{i})} A(t_\mathrm{s}-\tau,t_\mathrm{i}-\tau)}_{\substack{\text{signal = long arm}\\ \text{idler = long arm}}} - \underbrace{\mathrm{e}^{\mathrm{i}\varphi_\mathrm{s}} A(t_\mathrm{s}-\tau,t_\mathrm{i})}_{\substack{\text{signal = long arm}\\ \text{idler = short arm}}} - \underbrace{\mathrm{e}^{\mathrm{i}\varphi_\mathrm{i}} A(t_\mathrm{s},t_\mathrm{i}-\tau)}_{\substack{\text{signal = short arm}\\ \text{idler = long arm}}} \Bigg|^2, \end{aligned} \tag{4}$$

where $|\psi\rangle$ and $A(t_s,t_i)$ are given in Eq. (1). We point out that only the first 2 terms (both photons enter the short arms, or the long arms, of their respective MZIs) of Eq. (4) give rise to interference.

The parameters for the simulation are given in Table 1; these parameters are chosen as they correspond to our experimental values (See Section 3). Figures 2(b) and 2(c) show the simulated intensity plot of the coincidence rates, with $R(t_s,t_i)$ (z-axis) plotted as a function of the signal (t_s) and idler (t_i) arrival times. Interference can only occur when the signal and idler photons enter the same arms of their respective MZIs (first 2 terms of Eq. (4)). Moreover, even when both photons of a photon pair enter the short (long) arms of the MZI, there is only a small region of interest (denoted by the white box in Figs. 2(b) and 2(c), and region of interest (ROI) in Table 1) where their temporal wavefunctions overlap. When the relative phase of the interferometer is varied from 0 (Fig. 2(b)) to 180° (Fig. 2(c)), constructive interference changes to fully destructive interference, with the coincidence rate in the ROI vanishing as a result.

There are two inequalities that are present in the definition of the ROI (Table 1). The first, $|t_s - t_i| \leqslant 100$ ps, is used to exclude the coincidence counts resulting from the signal and idler photons entering opposite arms of their respective interferometers (third and fourth terms of Eq. (4)). As for the second inequality, $|t_s + t_i - \tau| \leqslant t_{\mathrm{ROI}}$, the parameter t_{ROI} allows us to adjust the region of overlap

Table 1 Simulation (and experimental) parameters

parameter	symbol	value
MZI imbalance	τ	500 ps
(characteristic) pulsewidth	τ_h	300 ps
single photon bandwidth	Δ	124 GHz
signal photon arrival time	t_s	variable
idler photon arrival time	t_i	variable
region of interest	ROI	$\lvert t_\mathrm{s}-t_\mathrm{i}\rvert \leqslant 100\,\mathrm{ps}$, $\lvert t_\mathrm{s}+t_\mathrm{i}-\tau\rvert \leqslant t_{\mathrm{ROI}}$, with t_{ROI} = 100 ps

to maximize interference visibility. The choice for t_{ROI}, however, is not arbitrary. Let us define a coincidence rate $\tilde{R}(t_{\mathrm{s}},t_{\mathrm{i}})$ that includes only the terms in Eq. (4) that give rise to interference, i.e., where both signal and idler photons traverse the short (long) arms of their respective interferometers:

$$\begin{aligned}\tilde{R}(t_{\mathrm{s}},t_{i}) &= |A(t_{\mathrm{s}},t_{\mathrm{i}}) + \mathrm{e}^{\mathrm{i}(\varphi_{\mathrm{s}}+\varphi_{\mathrm{i}})}A(t_{\mathrm{s}}-\tau,t_{\mathrm{i}}-\tau)|^2 \\ &= |A(t_{\mathrm{s}},t_{\mathrm{i}})|^2 + |A(t_{\mathrm{s}}-\tau,t_{\mathrm{i}}-\tau)|^2 \\ &\quad + 2\mathrm{Re}[\mathrm{e}^{-\mathrm{i}(\varphi_{\mathrm{s}}+\varphi_{\mathrm{i}})}A(t_{\mathrm{s}},t_{\mathrm{i}})A^{*}(t_{\mathrm{s}}-\tau,t_{\mathrm{i}}-\tau)].\end{aligned}$$

This expression is essentially the post-selected coincidence rate used in the conventional Franson interferometer [3]. Assuming that $A(t_{\mathrm{s}},t_{\mathrm{i}})$ is symmetric about its peak, we can show that the fringe visibility V of the interference can be written as

$$V = \frac{\iint_{\mathrm{ROI}} A(t_{\mathrm{s}},t_{\mathrm{i}})A^{*}(t_{\mathrm{s}}-\tau,t_{\mathrm{i}}-\tau)\mathrm{d}t_{\mathrm{s}}\mathrm{d}t_{\mathrm{i}}}{\iint_{\mathrm{ROI}} |A(t_{\mathrm{s}},t_{\mathrm{i}})|^2\mathrm{d}t_{\mathrm{s}}\mathrm{d}t_{\mathrm{i}}}. \quad (5)$$

Our choice of ROI is chosen so as to maximize V, but still yield substantial ($>10\%$ of the original) coincidence rates. Given the values of τ_{h} and τ (Table 1), we can numerically calculate the visibility V as a function of t_{ROI} (Fig. 3). We observe that reducing the ROI improves the interference visibility. In fact, for the $\tau = 500$ ps trace, when $t_{\mathrm{ROI}} = 100$ ps, $V = 0.945$ is observed. On the other hand, as the ROI is expanded, the visibility decreases, approaching 0.23 asymptotically.

Figure 3 also plots the visibilities for cases where a shorter (τ = 250 ps, dotted line) and longer (τ = 750 ps, dashed line) MZI imbalance is used. For the shorter imbalance, since there is greater overlap between trailing and leading edges of the biphoton, V remains close to unity over a wider range of ROI values, never dropping below 0.68. On the other hand, a setup with a larger imbalance ($\tau = 750$ ps) can only reach unity visibility for small values of t_{ROI} (<50 ps), with V decreasing to 0.035 asymptotically for large t_{ROI}.

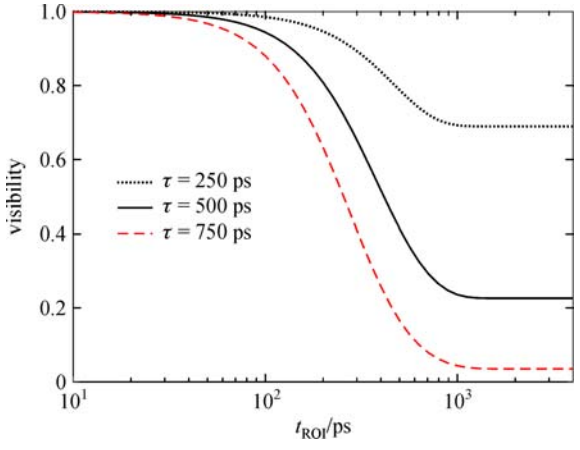

Fig. 3 Interference visibility V of our interferometer is plotted as a function of the ROI size t_{ROI} for various MZI imbalance values τ; the pulsewidth τ_{h} is kept constant (see Table 1). At τ = 500 ps, which corresponds to our experimental value, the visibility moves toward unity as the ROI becomes smaller ($V = 0.945$ is observed at t_{ROI} = 100 ps), and approaches an asymptotic value of 0.23 when the ROI increases

A key assumption we have made in this section (and in Eq. (1)) is that the pump pulse is transform-limited. That is, the frequency content along the temporal extent of the pulse does not change. If the pump pulse is chirped, however, the photon pairs generated by the leading and trailing edges of the pump pulse will become (at least partially) distinguishable, reducing interference visibility inside the ROI. In this way, our interferometer acts as a downconverted measure of the chirp of the pump pulse.

3 Experiment and results

Our experimental setup is similar to Fig. 1. An actively-modelocked Ti:sapphire laser, generating an 81.6 MHz pulse train of 460-ps (full width at half-maximum, FWHM) pulses at a central wavelength of 776.3 nm, is used as the pump. This FWHM pulsewidth corresponds to a characteristic pulsewidth τ_{h} of 300 ps in Eq. (1). A fiber-based second-order nonlinear medium [10,11] downconverts the Ti:sapphire pulsetrain into photon pairs centered about 1552.6 nm. Frequency-conjugate wavelength-division multiplexing (WDM) filters centered about 1548.6 and 1554.6 nm with 1 nm FWHM ($\Delta \sim 124$ GHz) are used to separate signal and idler photons (respectively). The MZIs used are temperature-stabilized planar-lightwave-circuit-based (PLC) devices that have an imbalance τ of 500 ps. The relative phase of the two arms of each MZI can be adjusted using a thermo-optic phase-shifter (φ_{s}, φ_{i}) in its long arm.

Free-running single photon detectors (SPDs, idQuantique 220) placed at the output of each MZI are used to measure the arrival times of the signal and idler photons with respect to the pump pulse. A PicoQuant Hydraharp 400 time interval analyzer (TIA) is run in T3 mode to time-tag all detector clicks with respect to the Ti:sapphire sync signal at a resolution of 32 ps. The pump power is chosen so that approximately 10^{-2} pairs/pulse are generated. The downconverted photon pairs are then routed to MZIs with imbalance $\tau = 500$ ps.

When the relative phase $\varphi_{\mathrm{s}} + \varphi_{\mathrm{i}}$ of the interferometer is 0, we observe in Fig. 4(a) that the biphotons generated by the trailing and leading edge of the pump pulse add constructively (bright spot at $t_{\mathrm{s}} = t_{\mathrm{i}} = \dfrac{\tau}{2} = 250$ ps). Likewise, when $\varphi_{\mathrm{s}} + \varphi_{\mathrm{i}} = 180^{\circ}$, there is destructive interference, and a node is present at $t_{\mathrm{s}} = t_{\mathrm{i}} = 250$ ps (Fig. 4(b)). Contrasting these experimental results with the

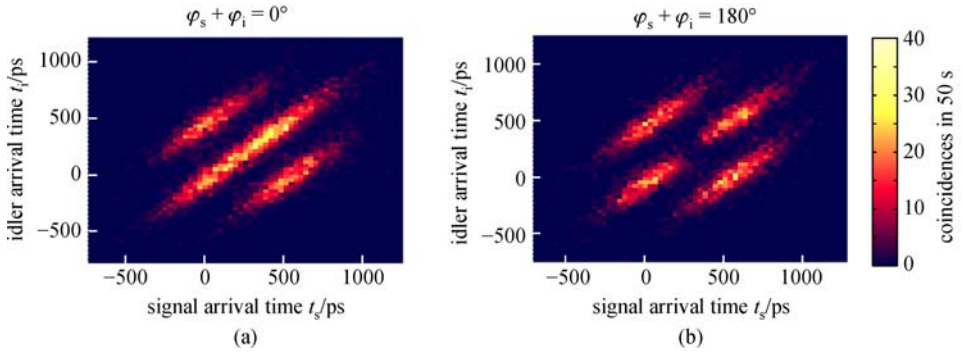

Fig. 4 Experimentally-obtained coincidence intensity plot. Antinode (a) and node (b) are observed when the relative phase of the interferometer is varied from 0° to 180°

simulated data (Figs. 2(b) – 2(c)), we see good qualitative agreement.

In order to extract the interference visibility, we vary the phase of the interferometer over a full 360°, and post-select only the coincidence counts where we expect the interference to occur from the intensity plot. If we take the approached used in the conventional Franson interferometry (Fig. 5(a)), where the entirety of the short-short and long-long events are summed up (Fig. 5(a) inset), the visibility is low (22.1 %), but in good agreement with theory (see Fig. 3). However, if we isolate ourselves to the ROI (Table 1, Fig. 5(b) inset) where the biphotons are expected to overlap temporally, the observed visibility is significantly greater (89.8%, Fig. 5(b)).

We recognize that a source of noise that contributes to the lower interference visibility is the jitter of the SPDs used, measured to be 120 ps (FWHM) (Fig. 6). The presence of this jitter means that the measured photon arrival times are smeared out over 120 ps or more. A 2-D point-spread function (PSF) can be obtained from the measured finite response of the detectors (Fig. 6). By removing (deconvolving) out this PSF from the coincidence plots (Fig. 4), we are able to obtain higher interference visibility. The algorithm used for this deconvolution is the iterative Richardson-Lucy method [12], which allows for the maximum-likelihood recovery of the original image before convolution with a known PSF. The results of deconvolution are shown in Fig. 7(a), along with the recovered fringe visibility (Fig. 7(b)), which is now near-unity (97.4 ± 4.3%). Once again, this value is in good agreement with our theoretical prediction of 94.5% (see Section 2).

The near-unity fringe visibility tells us that the photon pairs generated by both the trailing and leading edges of the pump are indistinguishable from each other. We can infer from this that the pump pulsetrain used is transform-limited.

4 Conclusions

In summary, we have demonstrated a new type of Franson interference. Instead of the conventional method involving a long coherence pump, or the time-bin method involving coherent pulsetrains, we showed that it is possible for photon pairs generated by the leading and trailing edges of

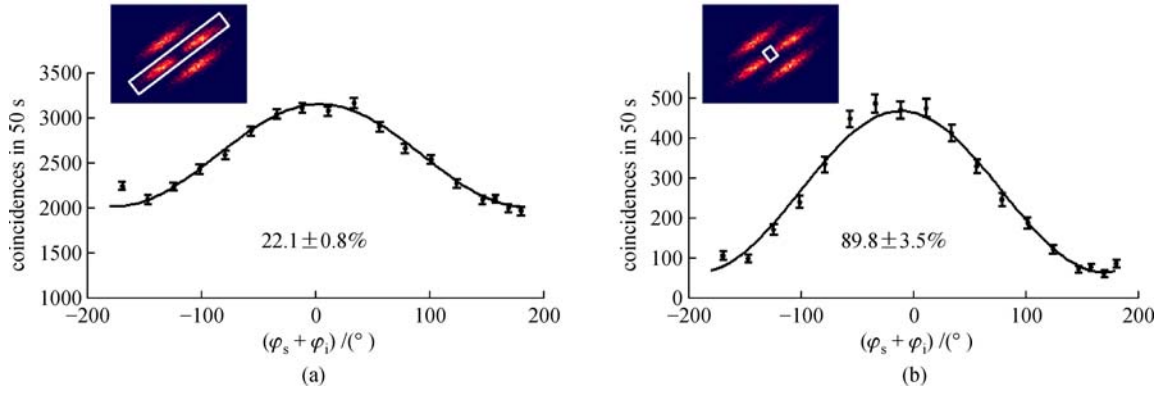

Fig. 5 Effect of post-selection on the interference visibility. The insets show the regions of the coincidence intensity plots used to extract the interference fringes. (a) When the temporally post-selected region includes the entirety of the short-short and long-long events, a low visibility of 22.1% is observed. (b) However, when only the ROI (Table 1) is post-selected, a significantly greater visibility (89.8%) is observed

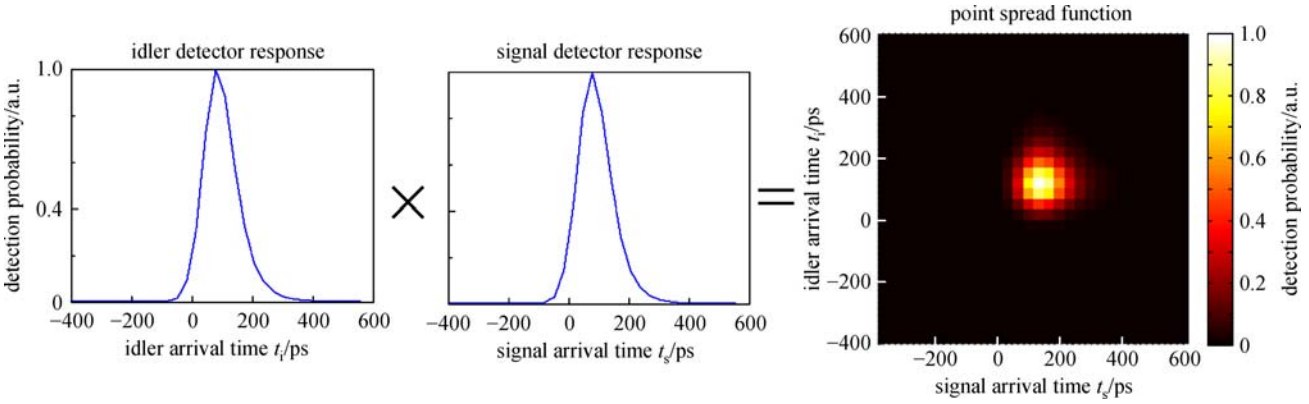

Fig. 6 Point spread function of our measurement system (single photon detectors and time-interval analyzer)

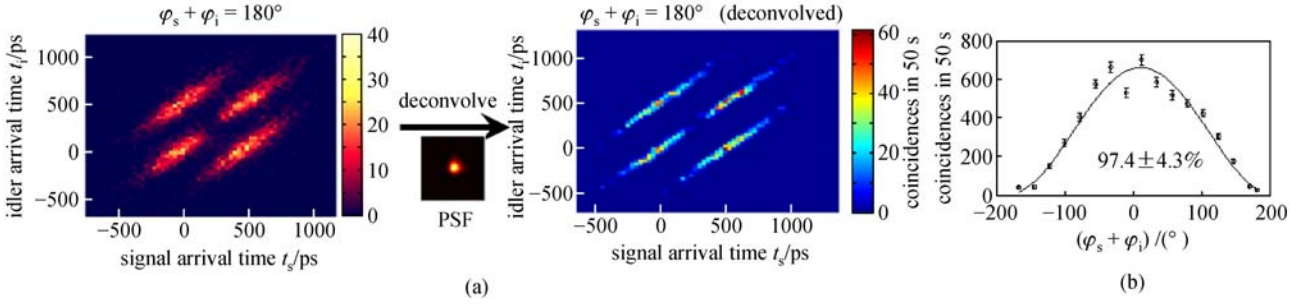

Fig. 7 (a) Deconvolving out the PSF reveals a coincidence intensity plot with finer features; (b) these finer features result in much higher, near-unity fringe visibilities

the same pulse to interfere. Furthermore, we have shown that the finite timing jitter of our SPDs can be accounted for and removed via numerical deconvolution, revealing near-unity (97.4%) interference visibility. This work may pave the way for the encoding and recovery of higher-dimensional quantum information from a single pulsed biphoton.

References

1. Hong C K, Ou Z Y, Mandel L. Measurement of subpicosecond time intervals between two photons by interference. Physical Review Letters, 1987, 59(18): 2044–2046
2. Patel R B, Bennett A J, Farrer I, Nicoll C A, Ritchie D A, Shields A J. Two-photon interference of the emission from electrically tunable remote quantum dots. Nature Photonics, 2010, 4(9): 632–635
3. Franson J D. Bell inequality for position and time. Physical Review Letters, 1989, 62(19): 2205–2208
4. Kwiat P G, Steinberg A M, Chiao R Y. High-visibility interference in a Bell-inequality experiment for energy and time. Physical Review A, 1993, 47(4): R2472–R2475
5. Ali-Khan I, Broadbent C J, Howell J C. Large-alphabet quantum key distribution using energy-time entangled bipartite states. Physical Review Letters, 2007, 98(6): 060503-1–060503-4
6. Bell J S. On the Einstein-Podolsky-Rosen paradox. On The Foundations of Quantum Mechanics. Singapore: World Scientific Publishing Co., 2001, 7–12
7. Marcikic I, de Riedmatten H, Tittel W, Scarani V, Zbinden H, Gisin N. Time-bin entangled qubits for quantum communication created by femtosecond pulses. Physical Review A, 2002, 66(6): 062308-1–062308-6
8. Hayat A, Xing X, Feizpour A, Steinberg A M. Multidimensional quantum information based on single-photon temporal wavepackets. Optics Express, 2012, 20(28): 29174–29184
9. Glauber R J. Coherent and incoherent states of the radiation field. Physical Review, 1963, 131(6): 2766–2788
10. Zhu E Y, Tang Z, Qian L, Helt L G, Liscidini M, Sipe J E, Corbari C, Canagasabey A, Ibsen M, Kazansky P G. Poled-fiber source of broadband polarization-entangled photon pairs. Optics Letters, 2013, 38(21): 4397–4400
11. Chen C, Zhu E Y, Riazi A, Gladyshev A V, Corbari C, Ibsen M, Kazansky P G, Qian L. Compensation-free broadband entangled photon pair sources. Optics Express, 2017, 25(19): 22667–22678
12. Richardson W H. Bayesian-based iterative method of image restoration. Journal of the Optical Society of America, 1972, 62 (1): 55–59

Eric Y. Zhu received his bachelor's degree in engineering physics and Ph.D degree in electrical engineering from the University of Toronto. He received further postdoctoral training at the National Institute of Standards and Technology, Gaithersburg, Maryland, USA. His current research interests include quantum optics, laser spectroscopy, and biophotonics.

Costantino Corbari graduated from the University of Milan, Faculty of Physics, with a thesis on electronic speckle pattern interferometry under the supervision of Prof. M. Giglio. In 2001 he was awarded a PhD scholarship by Pirelli cables & systems and went on to obtain his Ph.D. degree from the Optoelectronics Research Centre in Southampton, UK. He worked at the ORC within Prof. P. G. Kazansky's physical optics group until April 2015. Costantino has authored or co-authored 89 research papers encompassing laser interferometry, laser machining in glass, non-linear optics and the physics and applications of glass poling. He designed and built a precision laser machining workstation for the fabrication of 30-cm long periodically poled fibres. His non-linear fibre devices have been used as a source of entangled photons and for the demonstration of all-fibre frequency doubled lasers producing in excess of 2W second-harmonic average power from a single poled fibre. Throughout his career, Costantino had the pleasure of learning several optical techniques and developed a keen interest in their application. Costantino currently works for the metrology company Renishaw where he leads the Optical Systems team in the Laser and Calibration Product Division. He continues to pursue his interests in optical engineering and contributes to the design and verification of Renishaw's multi-axis laser calibrators and laser-encoders products range.

Alexey V. Gladyshev received the B.S. and M.S. degrees in laser physics from the Moscow Institute of Physics and Technology, Dolgoprudny, Russia, in 2001, and the Ph.D. degree in laser physics from the Fiber Optics Research Center, Russian Academy of Sciences, Moscow, Russia, in 2005. Since 2005, he has been with the Fiber Optics Research Center, Moscow, as a senior research scientist. His interests include fiber optics, nonlinear optics, and quantum optics.

Peter G. Kazansky studied physics in Moscow State University and received the Ph.D. degree from the General Physics Institute (GPI) in 1985. From 1989 to 1993 he led a group in the GPI, which unravelled the mystery of light-induced frequency doubling in glass. In 1992 he joined the ORC at the University of Southampton where since 2001 he is a professor pursuing his interests in new optical materials and phenomena including glass and fiber poling. More recently he pioneered the field of ultrafast laser nanostructuring in glass leading to invention of "5D memory crystal", which holds a Guinness world record for the most durable data storage medium. From 2014 he is also a director of the International Centre of Laser Technologies in Mendeleev University of Chemical Technologies. He is a Fellow of the Optical Society of America.

Li Qian (Ph.D., University of Toronto) is currently a professor in the Department of Electrical and Computer Engineering, University of Toronto. Her research focuses on novel fibre-optic devices and systems, including fibre sensing, nonlinear fibre optics and quantum optical sources based on periodically poled fiber. She also works on experimental quantum key distribution systems over fibre networks.